Supplementary Information

Sub-microsecond 2D Molecular Motion Mapping of Polymer Resin Enabled by Machine Learning

Masahiro Kuramochi,[1*] Kentaro Hoshisashi,[2] Shunya Shimomura,[3] Daisuke Sasaki,[3] Tatsuya Arai,[3] Kazuhiro Mio,[4] Hiroshi Sekiguchi,[5] Kentaro Uesugi,[5] Yoshio Suzuki,[3] Shotaro Akaho,[6,7] Yuji C. Sasaki[3, 4, 5*]

[1]Graduate School of Science and Engineering, Ibaraki University, Hitachi, 316-8511, Japan

[2]Department of Computer Science, University College London, Gower Street, London, WC1E 6BT, UK

[3]Graduate School of Frontier Sciences, The University of Tokyo, Kashiwa, 277-8561, Japan

[4]AIST-UTokyo Advanced Operando-Measurement Technology Open Innovation Laboratory (OPERANDO-OIL), National Institute of Advanced Industrial Science and Technology (AIST), Kashiwa, 277-0882, Japan

[5]Center for Synchrotron Radiation Research, Japan Synchrotron Radiation Research Institute, 1-1-1, Kouto, Sayo-cho, Sayo-gun, Hyogo, 679-5198, Japan

[6]The Institute of Statistical Mathematics, Tachikawa, 190-8562, Japan

[7]National Institute of Advanced Industrial Science and Technology, Tsukuba, 305-8568, Japan

Corresponding Author

Masahiro Kuramochi, masahiro.kuramochi.vw26@vc.ibaraki.ac.jp

Yuji C. Sasaki, ycsasaki@edu.k.u-tokyo.ac.jp

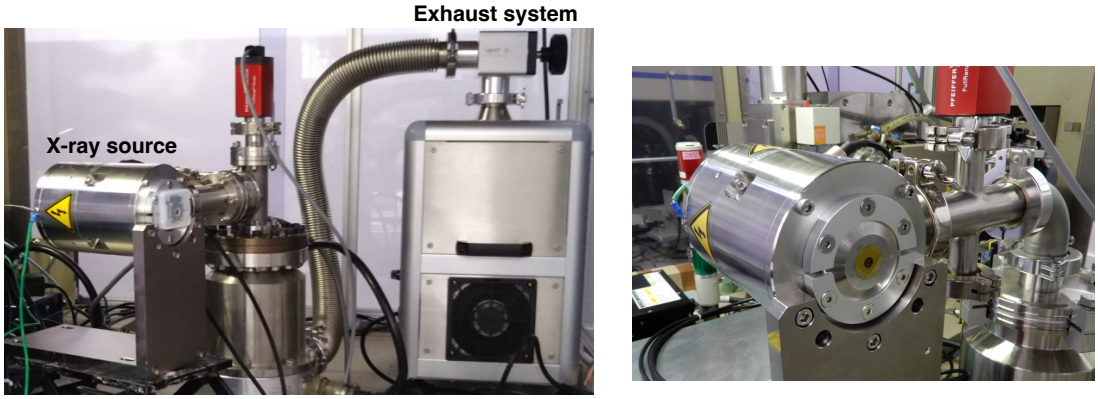

Figure S1. Laboratory X-ray source and experimental setup for TXB measurement.

Photographs of the compact laboratory X-ray source (left and right) and exhaust system (left) used for TXB experiments. The system consists of a Cu anode X-ray tube (wavelength = 1.54 Å) and an integrated exhaust unit to ensure safe and stable operation. The setup enables high-speed time-resolved X-ray transmission imaging with sub-microsecond temporal resolution.

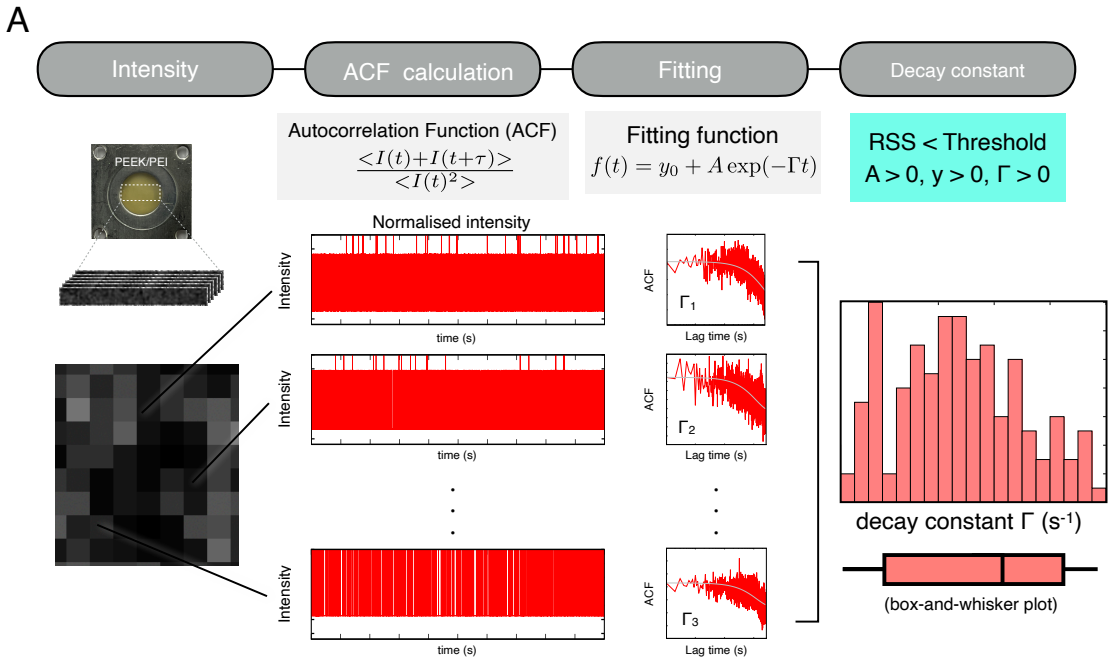

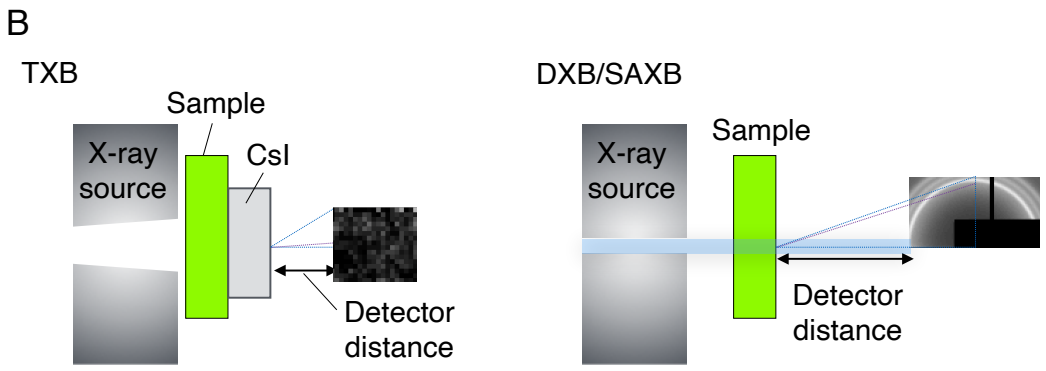

	Wavelength [Å]	detector distance [mm]	pixel size [μm²]	2θ [°]	d [nm]	Median value of decay constant [s⁻¹]		Rotational diffusion [nm²/s]		
TXB	1.54	3	20 x 20	3.05 - 0.38	2.89 - 23.22	**PEEK**	647.83	1.35E+03	—	8.73E+04
						PEI	602.27	1.26E+03	—	8.12E+04
SAXB	1.54	150	172 x 172	5.96 - 0.59	1.48 - 14.82	**PEEK**	0.0014	7.67E-04	—	7.69E-02
						PEI	0.0016	8.76E-04	—	8.79E-02
DXB	1.54	15	172 x 172	33.6 - 26.7	0.27 - 0.33	**PEEK**	0.0051	9.29E-05	—	1.39E-04
						PEI	0.0042	7.65E-05	—	1.14E-04

Figure S2. Schematic illustration of spACF analysis and the detection range in TXB measurements.

(A) Workflow of ACF-based analysis. Pixel-wise normalized intensity profiles were subjected to autocorrelation function (ACF) analysis. Each ACF curve was fitted with a single-exponential function to extract the decay constant (Γ). Only decay constants that met predefined criteria (positive amplitude, positive baseline, positive decay constant,

and residual sum of squares below a threshold) were retained for further evaluation. The dynamic behavior of the material was assessed from the resulting distribution of decay constants. (B) Schematic of the detection geometry. X-rays with a wavelength of 1.54 Å were used. The detector distance and pixel size used in each measurement are summarized in the table below. Based on these parameters, the 2θ angle, corresponding d-spacing, and rotational diffusion coefficients were calculated.

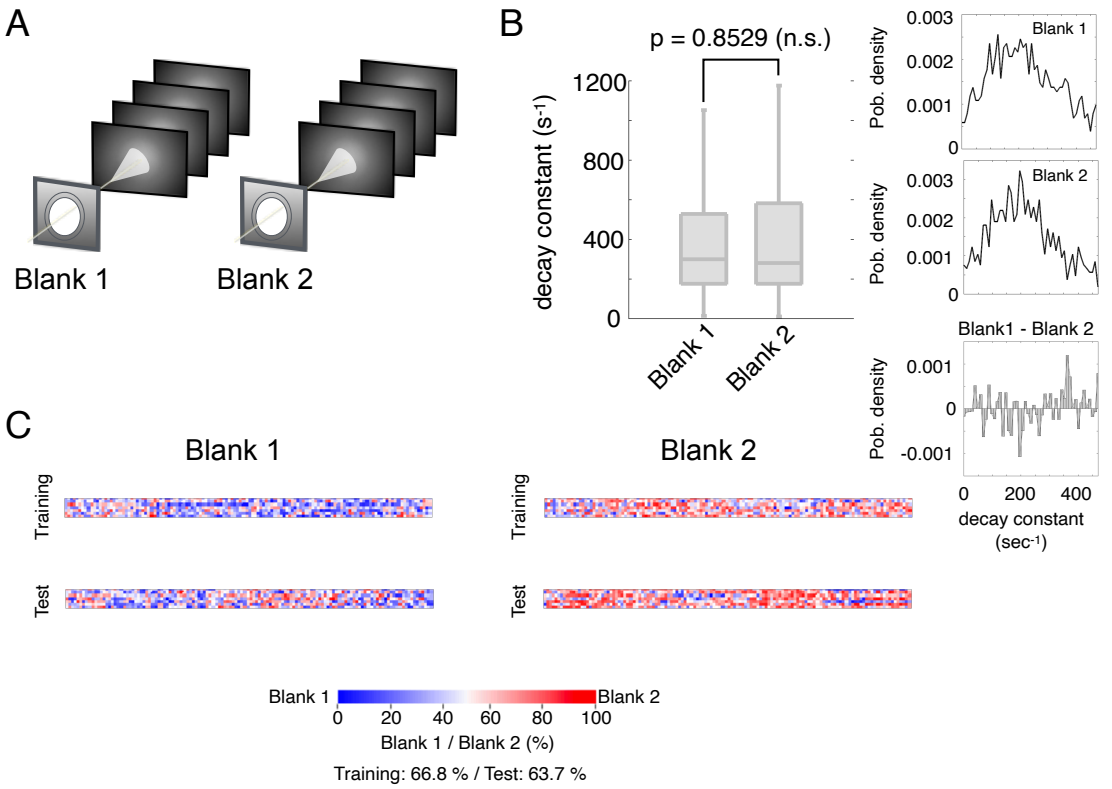

Figure S3. Control analysis using blank (no-sample) X-ray transmission movies. (A) Schematic representation of the two blank datasets (Blank 1 and Blank 2), captured under identical conditions with no sample present. (B) Comparison of ACF decay constant distributions between Blank 1 and Blank 2. Boxplots (left) show no statistically significant difference between the two conditions (p = 0.8529, n.s.). Probability density distributions of decay constants (right) were also highly similar, with their difference fluctuating around zero. (C) Results of machine learning–based classification between Blank 1 and Blank 2 using the same PCA–LDA pipeline as in the main experiment. The classification accuracy was low (Training: 66.8%, Test: 63.7%), suggesting that the high classification performance observed for PEEK vs. PEI is unlikely to arise from background fluctuations or system noise.

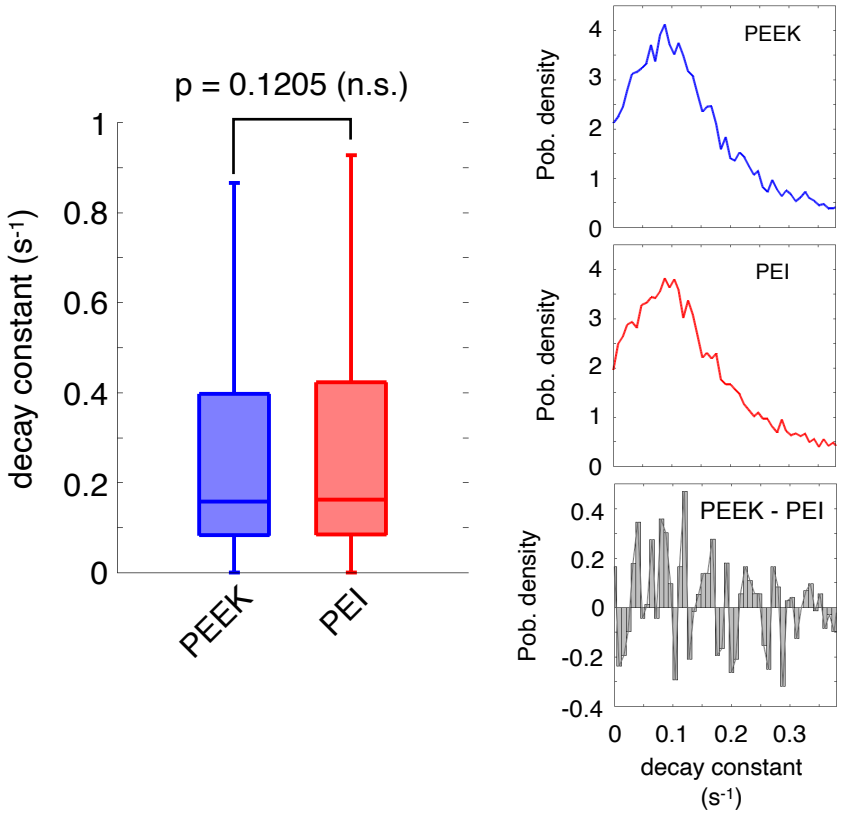

Figure S4. Comparison of ACF decay constants between PEEK and PEI at 5 ms/frame TXB measurement.

Boxplots (left) and probability density plots (right) show no statistically significant difference in decay constants between PEEK and PEI ($p = 0.1205$, n.s.). This result is consistent with SAXB measurements (50 ms/frame), and contrasts with the clear differences observed at 900 ns/frame TXB, indicating the importance of high temporal resolution for detecting dynamic contrast.

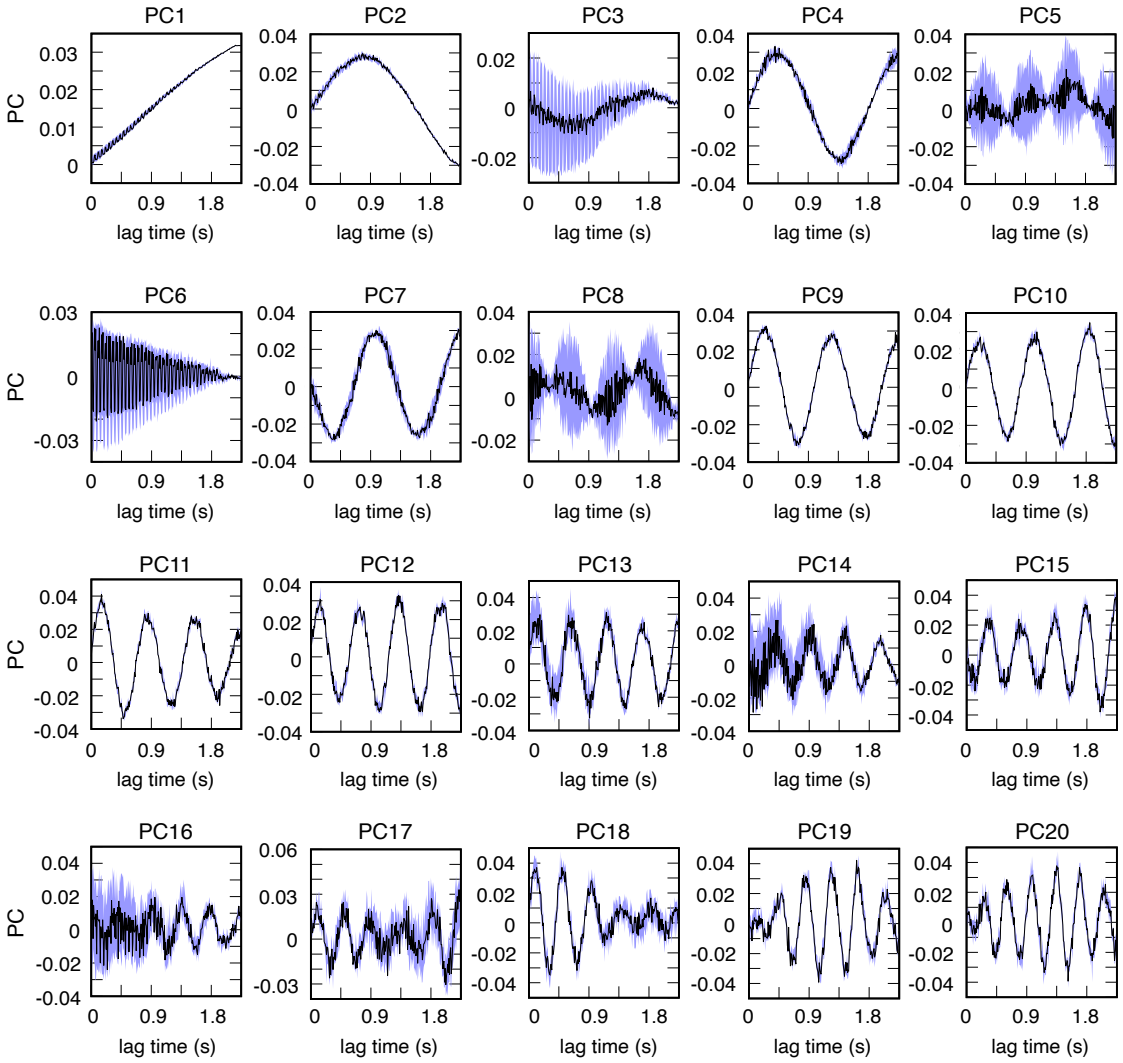

Figure S5. Temporal profiles of the top 20 principal components (PCs) derived from ACF data.

To simplify the visual representation of the 2500-frame time series, the data were divided into 250 segments (each comprising 10 frames). For each segment, three representative values—the preceding, central, and following points—were obtained. The central value is shown as a black line, while the adjacent values are shown as a blue band, representing the variability in the neighboring frames. PC1 primarily captures the decay trend, while higher-order PCs (e.g., PC4 and PC5) exhibit periodic-like oscillations, reflecting distinct dynamic features present in the dataset.

Table S1. Classification accuracy of PEEK and PEI based on five independent trials.

Each trial used a different subset of the data for training and testing in the LDA-based classification analysis. The training and test accuracies (%) are reported for each trial. The average accuracy and standard error across all trials are also shown.

No.	Training (%)	Test (%)
1	91.0	90.2
2	91.0	90.7
3	90.5	88.9
4	91.3	90.0
5	91.7	91.9
Average	91.1	90.3
Std. Error	0.4	1.1